Aircraft Maneuver Design Using Bifurcation Analysis and Sliding Mode Control Techniques

Article *in* Journal of Guidance, Control, and Dynamics · September 2012

DOI: 10.2514/1.56361

3 authors:

Amit Kumar Khatri
National Aerospace Laboratories
4 PUBLICATIONS **35** CITATIONS
SEE PROFILE

Jatinder Singh
National Aerospace Laboratories
3 PUBLICATIONS **34** CITATIONS
SEE PROFILE

Nandan K Sinha
Indian Institute of Technology Madras
53 PUBLICATIONS **237** CITATIONS
SEE PROFILE

JOURNAL OF GUIDANCE, CONTROL, AND DYNAMICS
Vol. 35, No. 5, September–October 2012

Aircraft Maneuver Design Using Bifurcation Analysis and Sliding Mode Control Techniques

Amit Kumar Khatri* and Jatinder Singh†
Council of Scientific and Industrial Research–National Aerospace Laboratories, Bangalore 560 017, India
and
Nandan Kumar Sinha‡
Indian Institute of Technology–Madras, Chennai 600 036, India

DOI: 10.2514/1.56361

In this paper, bifurcation analysis-based methodology is used in conjunction with a sliding-mode-based control algorithm to construct and simulate maneuvers for a nonlinear, 6 degree-of-freedom, F-18 high-alpha research vehicle aircraft model. Three different types of maneuvers, namely, a minimum-radius level turn, velocity vector roll, and spin recovery to a level flight condition, are attempted to demonstrate the usefulness of the proposed approach. The procedure involves constructing the desired maneuvers using constrained bifurcation analysis-based methodology. The results obtained from bifurcation analysis provide the reference inputs for the sliding mode controller to switch the aircraft between desired flight conditions. Robustness of the sliding mode controller is also examined by introducing uncertainties in aerodynamic parameters. Closed-loop simulation results are later presented to show the effectiveness of the proposed technique.

Nomenclature

b	=	wingspan, ft
C_D, C_L, C_Y	=	coefficients of drag, lift, and side force, respectively
C_l, C_m, C_n	=	aerodynamic rolling, pitching, and yawing moment coefficients, respectively
c	=	mean aerodynamic chord, ft
I_x, I_y, I_z	=	roll, pitch, and yaw moments of inertia, slug-ft^2
m	=	mass of aircraft, slug
n_z	=	load factor of aircraft
p, q, r	=	body axis roll, pitch, and yaw rates, respectively, rad/s
S	=	wing planform area, ft^2
T_m	=	maximum available engine thrust, lb
V	=	velocity of aircraft, ft/s
α, β	=	angle of attack and sideslip angle, respectively, rad
δ_e, δ_a, δ_r	=	elevator, aileron, and rudder angles, respectively, rad
η	=	thrust as a fraction of maximum available thrust
μ, γ	=	wind-axis angles, rad
ρ	=	air density, slug/ft^3
ϕ, θ	=	Euler bank and pitch angles, respectively, rad
Ω	=	velocity vector roll rate, rad/s
$\boldsymbol{\omega}$	=	angular velocity vector, rad/s

Subscripts

f	=	final trim point
i	=	initial trim point

Superscripts

T	=	transpose
γ_i	=	relative degree of the ith output variable

I. Introduction

MODERN day fighter aircraft are desired to possess extreme maneuvering capabilities, such as the ability to perform aggressive maneuvers in poststall flight regime. Any typical flight maneuver essentially entails transitioning the aircraft between different operating points lying within the bounded flight envelope of aircraft, while satisfying a set of constraints. For instance, a zero sideslip, level turn maneuver requires constraining the sideslip and flight path angles to zero. Design of constrained maneuvers has been a topic of great interest in recent times, with major effort being in the design of minimum-time or minimum-energy maneuvers in which a particular performance index is maximized or minimized. The basic maneuver design problem is usually formulated as a boundary value problem. In addition, a set of constraints is also imposed on state and/or control parameters. An optimal solution for the state and control parameters that satisfies the prescribed constraints is then obtained using various optimization algorithms, for example, steepest ascent method [1], nonlinear programming [2,3], genetic algorithms [4], and direct transcription methods [5]. A different approach based on constrained bifurcation analysis-based methodology has been followed in this paper for constructing aircraft maneuvers.

Application of bifurcation analysis and continuation technique-based methodology for studying complex nonlinear aircraft flight dynamics phenomena was first demonstrated by Carroll and Mehra [6]. The technique has now evolved into a reliable tool for analyzing global dynamics of nonlinear aircraft models. Several nonlinear dynamic phenomena occurring in aircraft flight dynamics, such as high-α spin, deep stall, stall dynamics, wing rock, and inertia coupled rolling motions are now well explained and understood by the application of this technique [7–10]. A bifurcation analysis-based approach was implemented in [11] to demonstrate the possibility of achieving symmetric flight up to high incidence angles by modifying the spin behavior of an aircraft. Extensions of bifurcation analysis and continuation technique-based methodology for analyzing nonlinear flight dynamics under constrained motion were proposed in [12,13]. Nonlinear flight dynamics of closed-loop aircraft models, augmented with the control law of aircraft, were examined using this

Received 22 September 2011; revision received 18 February 2012; accepted for publication 21 February 2012.

*Scientist, Centre for Civil Aircraft Design and Development.
†Scientist, Flight Mechanics and Control Division. Senior Member AIAA.
‡Associate Professor, Department of Aerospace Engineering.

methodology in [14,15]. The technique was further explored for flight control law design: A global stability augmentation system employing linear feedback control strategy for suppressing wing rock motion was designed in [16]; interconnect laws and stability augmentation system were designed in [17] for avoiding bifurcation points in a straight and level flight condition; and a nonlinear dynamic inversion (NDI)-based controller was designed using the bifurcation analysis-based approach in [18]. Methods based on bifurcation analysis and continuation technique have also been used to compute "attainable equilibrium sets" that are helpful in comparing performance and maneuverability of different aircraft models [19]. Recently, bifurcation analysis-based methodology was used for examining nonlinear dynamic phenomena of a flexible aircraft model [20].

In recent years, use of feedback linearization-based nonlinear control techniques has found practical applications in aircraft flight dynamics, particularly in the areas of trajectory tracking control [3,21–23] and aircraft recovery from poststall conditions [24,25]. Among them, NDI and variable structure-based sliding mode control (SMC) techniques have been quite popular. Robustness of nonlinear controllers, however, has been a major issue with regards to their implementations in aerospace control applications. Although NDI-based controllers have been reported for their lack of robustness [26] and control saturation problems [25] (also observed by us), sliding mode controllers have been proven to be robust and have found wide applications in areas ranging from robotics to aerospace control. Comparison of two techniques in aerospace applications withstanding, to illustrate our proposed methodology for aircraft maneuver construction, we choose the SMC technique without loss of generality.

A brief review of SMC technique can be found in a survey paper by Utkin [27]. Controllers based on SMC technique for aircraft applications have been successfully demonstrated in the literature. SMC algorithm was formulated by Singh [28] for trajectory tracking in a lateral maneuver using a simplified seventh-order nonlinear aircraft model. SMC technique was used by Hedrick and Gopalswamy [29] to design a nonlinear pitch axis flight controller for tracking pilot g commands during a fast pull-up maneuver. Using SMC technique, a longitudinal flight controller was derived by Jafarov and Tasaltin [30] for a linear F-18 aircraft model with parametric uncertainties and external disturbance input. A nonlinear adaptive sliding mode controller was successfully designed in [23] for inertial trajectory tracking of aircraft maneuvers using a simplified F/A-18 aircraft model. Conditional integrator-based SMC for longitudinal motion control of F-16 aircraft was formulated in [31] using the concept of modal decomposition of longitudinal dynamics into short period and phugoid modes. Control allocation schemes based on SMC for design of fault-tolerant control systems have also been successfully attempted [32]. Recently, a controller based on SMC technique was designed for aircraft spin recovery [33]. In most of the earlier cited references on use of SMC technique in flight control law design, however, aircraft maneuvers were designed arbitrarily without considering the performance limits of the aircraft into account. Maneuvers, thus designed, do not exploit the full potential of aircraft. Constrained bifurcation analysis-based methodology equips the designer with a powerful tool to understand and assess the performance capabilities and maneuverability of the aircraft under various maneuver constraints. In this way, the maneuvers can be intelligently designed by having prior knowledge of the performance and maneuver characteristics of the aircraft.

The objective of this work is to present an efficient procedure for designing aircraft maneuvers by using constrained bifurcation analysis-based methodology and the SMC technique in conjunction. To demonstrate our approach, we first construct aircraft maneuvers using bifurcation analysis and continuation technique-based methodology. The technique involves imposing a set of constraints on a defined set of maneuver parameters and control parameters and carrying out a bifurcation analysis of the augmented nonlinear mathematical model of aircraft to obtain bifurcation plot for the model under specified constraints. The desired maneuver is then constructed by selecting the two trim points lying on the bifurcation plots between which the state trajectory of aircraft should be switched to achieve the maneuver; the choice of initial and final trim points being itself guided by the maneuver constraints. Next, a sliding mode controller for the regulation or tracking of desired controlled variables is designed. The controller is formulated by considering a complete eighth-order nonlinear aircraft model. The designed maneuvers are then simulated using the SMC controller in a closed-loop simulation by specifying numerical values of desired output variables of the selected trim points from bifurcation analysis as reference inputs to the controller. The results of closed-loop simulations presented in this paper demonstrate the usefulness of this combined approach.

The paper is organized in the following manner. Section II describes the procedure for construction of three example maneuvers, namely, a minimum-radius level turn, velocity vector roll and spin recovery to a level flight condition, followed by design of sliding mode controller in Sec. III. Section IV summarizes the results obtained through the proposed technique, and Sec. V concludes the paper.

II. Construction of Aircraft Maneuvers Using Bifurcation Analysis and Continuation Technique

Bifurcation analysis of a system governed by a set of nonlinear ordinary differential equations starts with computing all possible steady states of the system as a function of a varying parameter. This is usually done with the help of a continuation algorithm such as AUTO2000 [34], which also simultaneously computes stability of the steady states based on small perturbation criterion. As a result of this computation, one obtains what is popularly known as a "bifurcation diagram" or a map that exhibits global dynamic behavior of the system with respect to the continuation parameter. A major shortcoming of the standard bifurcation procedure as noted by Ananthkrishnan and Sinha [13] was that it allowed only one parameter of the system to vary in a continuation and thus could be termed as one-parameter bifurcation analysis. In a real-world scenario, a system usually operates under conditions that are constrained and multiple controls of the system are varied simultaneously to meet the criteria defined by the constraints. To study global dynamics of nonlinear dynamic systems in constrained conditions, a two-step methodology known as the extended bifurcation analysis (EBA) methodology was proposed in [13].

The EBA methodology consists of two steps. In the first step, equations of rigid-body flight dynamics along with the relevant constraint equations are solved simultaneously. These equations can be represented in vector form as

$$\dot{\mathbf{x}} = \mathbf{f}(\mathbf{x}, u, \mathbf{p}) = 0 \tag{1}$$

$$\mathbf{g}(\mathbf{x}) = 0 \tag{2}$$

where $\mathbf{x} = [V, \alpha, \beta, p, q, r, \phi, \theta]^T \in X \subset \Re^8$ is the vector of state variables, and $u \in U \subset \Re$ is the principal continuation parameter. The vector function $\mathbf{g}(\mathbf{x})$ represents a vector of constraints, and vector $\mathbf{p}$ denotes a bounded set of available control parameters. It is necessary that the number of control parameters in $\mathbf{p}$ should at least be equal to the number of imposed constraints for the constrained bifurcation analysis problem to be well posed, the other necessary condition being that constraints must influence the control parameters of the system so that they are strongly coupled. What it means is, in a continuation, a control parameter must change to satisfy a constraint equation. These necessary conditions can generally be satisfied for a well-formulated aircraft control problem. To perform the constrained bifurcation analysis of the augmented system of Eqs. (1) and (2), a set of control parameters (equal to the number of constraint equations) from $\mathbf{p}$ are freed and the remaining controls are held fixed. When there are multiple controls available for satisfying a desired constraint equation, a weighting function or influence coefficient is required to be computed to identify the most suitable candidate control parameter that should be released.

To illustrate the procedure for identifying the suitable control parameters for satisfying the imposed constraints, we consider a constant load factor, zero sideslip, level turn maneuver. Thus, the constraint set is

$$\gamma = 0; \qquad \beta = 0; \qquad \mu = \mu_c \tag{3}$$

where $\mu = \mu_c$ is a constant. The elevator is used as a principal continuation parameter, and $\mathbf{p} = [\eta, \delta_a, \delta_r]$ constitutes a vector of available control parameters.

Now, to identify the effective control parameter for satisfying the zero sideslip constraint, substitute for constraints (3) in the equation for time evolution of β (see the Appendix). Thus,

$$\dot{\beta} = \frac{1}{mV}\left[\frac{1}{2}\rho V^2 S C_Y(\alpha, p, r, \delta_a, \delta_r) + mg \ \sin\mu_c\right] + (p \ \sin\alpha - r \ \cos\alpha) \tag{4}$$

which can be rewritten as

$$\dot{\beta} = w_{\beta 1}(\alpha, V)\delta_a + w_{\beta 2}(\alpha, V)\delta_r + [\text{terms without } \mathbf{p}] \tag{5}$$

where $w_{\beta 1}$ and $w_{\beta 2}$ represent the influence coefficients for aileron and rudder, respectively. Because Eq. (5) contains both δ_a and δ_r control parameters, in principle, either of the two controls can be released to satisfy the zero sideslip constraint. However, a more effective of the two control parameters is generally chosen based on the relative magnitude of the two weights $w_{\beta 1}$ and $w_{\beta 2}$.

Again, substitute for constraint set (3) in the equation for $\dot{\gamma}$. Hence,

$$\dot{\gamma} = \frac{1}{mV}\left[T_m \eta\{\sin\alpha \ \cos\mu_c\} + \frac{1}{2}\rho V^2 S C_L(\alpha, q)\cos\mu_c - mg - \frac{1}{2}\rho V^2 S C_Y(\alpha, p, r, \delta_a, \delta_r)\sin\mu_c\right] \tag{6}$$

It can be noted that all the three available control parameters $(\eta, \delta_a, \delta_r)$ are explicitly present on the right-hand side of Eq. (6). Hence, any one of the three control parameters from control vector $\mathbf{p}$ can be freed to satisfy the flight path angle constraint. In general, it is the engine throttle η that is used to regulate the flight path angle. However, when either the engine throttle is intended to be kept fixed or if it saturates, then any one of the two remaining control parameters from $\mathbf{p}$ can be used to hold the flight path angle to the desired value.

To check for the effective control parameter that satisfies the constraint on the wind-axis roll angle, replace for the values of constraints (3) in the $\dot{\mu}$ equation. This, on simplification, reduces to

$$\dot{\mu} = p \ \cos\alpha + r \ \sin\alpha \tag{7}$$

Thus, none of the control parameters appears on the right-hand side of Eq. (7). So, differentiate $\dot{\mu}$ with respect to time and take the time derivatives of the three constrained variables as zero in the $\ddot{\mu}$ equation. Substituting for the constraints (3) in the resulting expression gives

$$\ddot{\mu} = (\dot{p} \ \cos\alpha + \dot{r} \ \sin\alpha) + (-p \ \sin\alpha + r \ \cos\alpha)\dot{\alpha} \tag{8}$$

After substituting for the expression of $\dot{p}$, $\dot{r}$, and $\dot{\alpha}$ in Eq. (8) along with the values of three constraints from Eq. (3), it can be noted that all the three controls from $\mathbf{p}$ appear explicitly in the expression for $\ddot{\mu}$. Hence, any one of the three control parameters can be used to satisfy the μ-constraint of expression (3). Again, for the augmented set of Eqs. (3), the number of constraints (three) and the number of available control parameters (three) are same, and all the control parameters satisfy the necessary condition of influencing at least one of the constraints. Hence, all the three parameters from vector $\mathbf{p}$ should be released to satisfy the specified constraint set.

The first step of the EBA methodology computes the set of all possible steady states satisfying the constraints imposed in Eq. (2). Parameter schedules for the freed parameters, as a function of continuation parameter u, thus become available as a solution of the first step. However, the stability information on the computed constrained steady states are incorrect because a continuation algorithm does not distinguish between the states and the free parameters. Also, the first step of EBA does not show any departure from the constrained flight conditions because the constraints are explicitly present in this step.

In the second step of the EBA methodology, parameter schedules for the freed parameters as determined from the first step are included in the aircraft model as

$$\dot{\mathbf{x}} = \mathbf{f}(\mathbf{x}, u, \mathbf{p_1}(u), \mathbf{p_2}) \tag{9}$$

In Eq. (9), vectors $\mathbf{p_1}$ and $\mathbf{p_2}$ refer to the free and fixed control parameters, respectively. Numerical continuation of the system of Eqs. (9) is now carried out with the parameter u varying as the continuation parameter; $\mathbf{p_1}$ varies as function of u in a particular manner so as to satisfy the constraints. Output of this step is the bifurcation diagram with correct stability information on the steady states. Instability and departure points, if any, from the constrained trim condition are also computed in the second step of the EBA methodology.

Three distinct maneuvers representing different flight objectives are now constructed in the following subsections using the EBA methodology. A full 6-DOF, rigid-body, nonlinear mathematical model (see the Appendix) of an F-18/high-alpha research vehicle (HARV) aircraft is used here for illustrating the technique. Tables A1 and A2 (see the Appendix) list the key aircraft data taken for this study. Geometrical parameters, mass and inertia characteristics, and the aerodynamic database used for F-18/HARV are same as that used in [25]. International Standard Atmosphere (ISA) sea level conditions are assumed for ambient atmospheric variables. All the bifurcation analysis results presented in this paper are obtained through publicly available AUTO2000 continuation and bifurcation software.

A. Minimum-Radius Level Turn Maneuver

In this maneuver, aircraft is required to perform a sustained horizontal loop of minimum radius at a constant speed and zero sideslip, starting from a straight and level flight condition. This maneuver requires information about the initial level, symmetric trim condition, and the final minimum-radius level turn trim states. A procedure has been described in [35] using the EBA technique to compute the maximum sustained turn rate of the aircraft. A similar procedure is adopted here to extract the minimum sustained turn radius states.

To determine the minimum sustained turn radius flight states, Eq. (1) is simultaneously solved with three different constraint sets as step 1 of EBA; the specified constraints are summarized in Table 1. These constraints essentially correspond to the propulsive, aerodynamic, and structural limits that determine the minimum turn radius of aircraft. The value of angle of attack for the maximum lift coefficient used in constraint set B of Table 1 is found from the $C_L - \alpha$ curve of aircraft shown in Fig. 1. The magnitude of bank angle in constraint C of Table 1 corresponds to the maximum permissible load factor of 5.4 for the structure of aircraft.

The first step of the EBA method is performed individually for all the three branches (A, B, and C) of Table 1, using elevator δ_e as the principal continuation parameter. Branch A solves for achievable level turn states with the maximum available engine thrust, hence, fraction of maximum throttle η is fixed at a value of 1. Because there are two constraints for branch A, the only two available parameters

Table 1 Summary of constraints

Branch	Constraints, $\mathbf{g}(\mathbf{x}) = 0$	Free parameters	Fixed parameters
A	$\gamma = 0, \beta = 0$	δ_a, δ_r	$\eta = 1.0$
B	$\gamma = 0, \beta = 0,$	δ_a, δ_r, η	——
	$\alpha = 0.62832$ rad $(=\alpha_{CL_{\max}})$	——	——
C	$\gamma = 0, \beta = 0,$	δ_a, δ_r, η	——
	$\mu = 1.3845$ rad $(n_z = 5.4)$	——	——

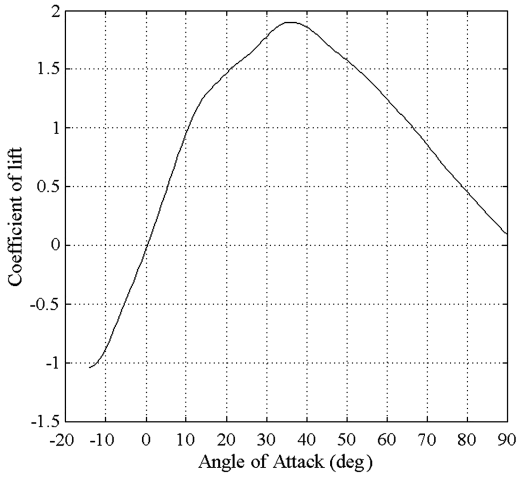

Fig. 1 Coefficient of lift C_L vs. angle-of-attack α curve for F-18/HARV.

(δ_a and δ_r) are freed: Both δ_a and δ_r were demonstrated in Eqs. (5) and (6) to influence the imposed constraints of Table 1. Branch B corresponds to level turn states possible at the maximum lift coefficient. To satisfy the three constraints for branch B, the only three available controls, η, δ_a, and δ_r, need to be released. Branch C gives solutions with maximum permissible load factor; the three controls η, δ_a, and δ_r are freed to satisfy the three imposed constraints of this branch.

Results of the first step of EBA provide the minimum sustained turn radius states and schedules for the free parameters. These schedules are subsequently used to analyze the stability of the steady states using the second step of EBA. Throttle schedules computed using the first step of EBA are shown in Fig. 2. It can be observed from the plots of Fig. 2 that throttle parameter η exceeds its limiting value of 1 on branches B and C. Hence, level turns are physically unrealizable on either of these two branches: Sustained turns can only be obtained on branch A. The bifurcation diagram computed from the second step of EBA is shown in Fig. 3. It can be noticed from Fig. 3 that minimum sustained turn radius flight is achievable at point "S" lying on branch A. At Point "CP," the corner point of aircraft, only an instantaneous turn of minimum radius can be flown.

The minimum-radius level turn states and corresponding trimming control inputs computed from the first step of EBA are

$$\mathbf{x}_f = [269.89, 0.37243, 0, 0.03289, 0.10726, -0.0842, -0.90534, 0.2367]^T \tag{10}$$

$$\eta = 1.0, \quad \delta_e = -0.1026, \quad \delta_a = 0.044, \quad \delta_r = 0.01338 \tag{11}$$

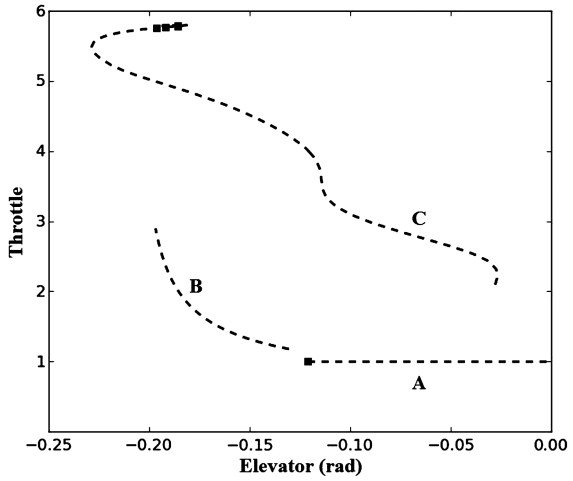

Fig. 2 Throttle schedules for the constraint set specified in Table 1 using the first step of EBA.

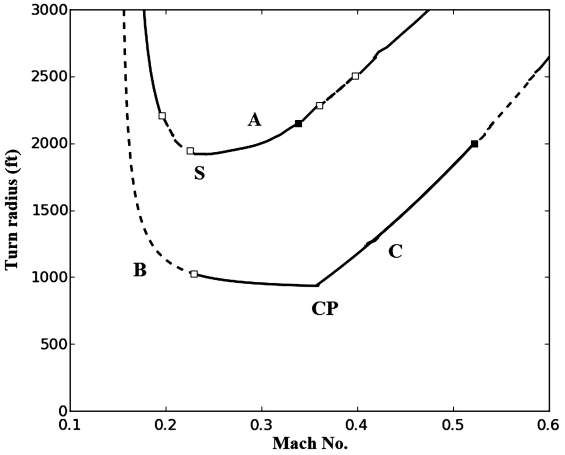

Fig. 3 Turn radius variation with Mach number; solid line, stable point; dotted line, unstable point; empty square, transcritical or pitchfork bifurcation; filled square, Hopf bifurcation.

From the bifurcation diagram depicted in Fig. 3, it can be noticed that the minimum sustained turn radius state represents an open-loop stable trim point. The stability of point S is also confirmed from the eigenvalues available from the computation of second step of EBA. The eigenvalues of point S are $[-0.00838, -0.0562 \pm 0.181\text{i}, -0.2502 \pm 0.5857\text{i}, -0.3023 \pm 2.072\text{i}, -0.4982]$.

The initial steady, level, symmetric flight trim states for the maneuver can be computed using the first step of EBA method by solving (1) with the following constraints:

$$\phi = 0, \qquad \gamma = 0, \qquad \beta = 0 \tag{12}$$

To perform EBA analysis, the elevator is used as a principal continuation parameter, and the three available controls (η, δ_a, and δ_r) are freed to satisfy the three constraints of Eq. (12). Results obtained from the first step of EBA are plotted in Fig. 4 in terms of the variation in Mach number with angle of attack.

Again, the minimum-radius level turn maneuver is desired to be performed at a constant speed, therefore, the velocity of initial steady, level, symmetric trim point should be same as that of the final trim point. From Fig. 4, point 1 is found to be the desired initial trim point. The state vector and control inputs for this initial operating point computed from the first step of EBA are

$$\mathbf{x}_{\text{i}} = [269.89, 0.1888, 0, 0, 0, 0, 0, 0.1888]^T \tag{13}$$

$$\eta = 0.3863, \qquad \delta_e = -0.0168, \qquad \delta_a = 0, \qquad \delta_r = 0 \tag{14}$$

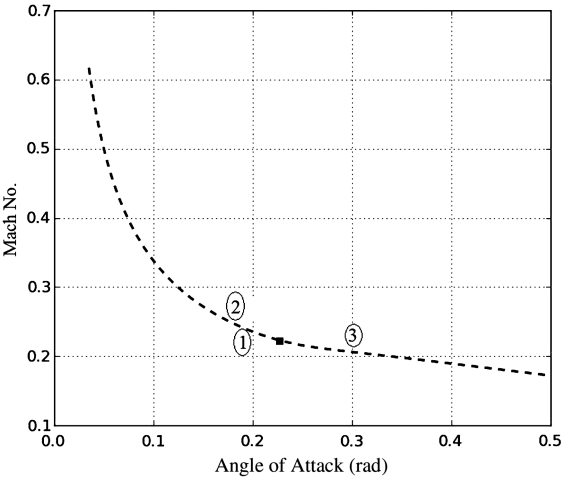

Fig. 4 Plot of Mach no. against angle of attack for steady, level, symmetric flight condition.

B. Velocity Vector Roll Maneuver

In a velocity vector roll (VVR) maneuver, the aircraft resultant angular velocity vector keeps pointing toward the instantaneous resultant velocity vector. The maneuver is often used by fighter aircraft pilots as a part of their combat strategy. VVR maneuver for ADMIRE aircraft model using NDI control law was demonstrated by Goman et al. [36]. The maneuver involved tracking a sinusoidal variation in velocity vector roll rate. In a later study, the attainable equilibrium set for a VVR maneuver at different ambient conditions (than used in our work) were computed for the F-18/HARV aircraft model using the bifurcation and continuation method [19]. The VVR maneuver constructed in this paper is motivated from [19,36].

In roll maneuvers, the effect of gravity is generally neglected and speed is assumed to be constant. Hence, a reduced fifth-order model is generally solved to obtain what are known as pseudo-steady-state solutions [7]. Additional constraints on angle of attack and sideslip angle are also employed here for the VVR maneuver. To compute the pseudo–steady states required for the VVR maneuver, the following set of equations are simultaneously solved:

$$\dot{\mathbf{x}} = \mathbf{f}(\mathbf{x}, u, \mathbf{p_1}, \mathbf{p_2}) = 0 \tag{15}$$

$$g_1(\mathbf{x}) = \alpha = 0.17453 \text{ rad} \tag{16}$$

$$g_2(\mathbf{x}) = \beta = 0 \tag{17}$$

For the set of Eqs. (15–17), the state vector $\mathbf{x} = [\alpha, \beta, p, q, r]$; $u = [\delta_a]$ is the principal continuation parameter; and $\mathbf{p_1} = [\delta_e, \delta_r]$ denotes the vector of free control parameters. There are no fixed control parameters in this case.

The EBA methodology is used here to simultaneously solve Eqs. (15–17) to extract the possible pseudo-steady-state solutions for the VVR maneuver; the aileron is used as the continuation parameter. The results obtained from the second step of the EBA method are shown in Figs. 5 and 6. The bifurcation diagrams are presented only for positive deflections of the continuation parameter; bifurcation plots for negative aileron deflections are similar to that shown in Figs. 5 and 6, but with reverse sign of values on the y axis. Figure 5 shows the rudder schedule required to achieve the constrained flight. It can be noticed from Fig. 5 that rudder input is very close to its deflection limit for a full aileron input. Bifurcation diagrams for velocity vector roll rate Ω and normalized velocity vector roll rate Ω_n are presented in Fig. 6, from which the maximum possible value of Ω under maneuver constraints (16) and (17) can be found. This information can now be effectively used to define the amplitude of Ω for the VVR maneuver, instead of arbitrary specifying the value of Ω.

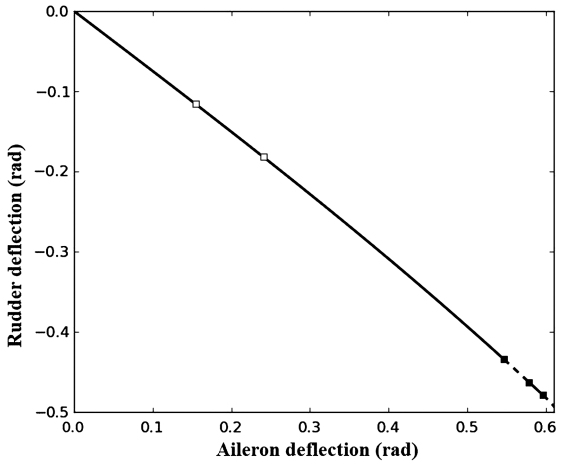

Fig. 5 Rudder schedule for VVR maneuver; solid line, stable point; dotted line, unstable point; empty square, key transcritical or pitchfork bifurcation; filled square, Hopf bifurcation.

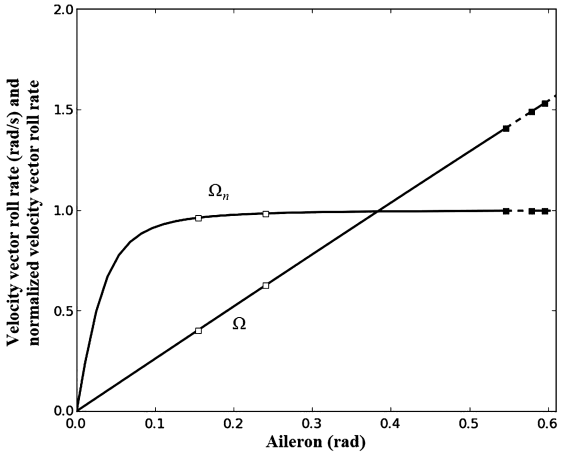

Fig. 6 Bifurcation diagram of VVR rate and normalized VVR rate using aileron as continuation parameter; see Fig. 5 for key to lines and symbols.

The parameters Ω and Ω_n shown in Fig. 6 are defined as

$$\Omega = \frac{\mathbf{V}.\boldsymbol{\omega}}{|\mathbf{V}|} \tag{18}$$

$$\Omega_n = \frac{\mathbf{V}.\boldsymbol{\omega}}{|\mathbf{V}||\boldsymbol{\omega}|} \tag{19}$$

where $\mathbf{V}$ represents the instantaneous velocity vector of aircraft.

The desired maneuver starts with the aircraft flying initially at a steady, level, symmetric flight condition. Aircraft is next commanded to perform a velocity vector roll while holding angle of attack to a constant value and restricting sideslip angle to zero. The parameters for the roll are

$$\Omega = \sin(0.2\pi t); \qquad \alpha = 0.17453 \text{ rad}; \qquad \beta = 0 \tag{20}$$

where the amplitude of Ω in roll has been restricted to 1.0 rad/s to avoid any plausible departure phenomena arising due to aileron and rudder surfaces saturation at higher values of Ω.

During the VVR maneuver, angle of attack is required to be held constant, and sideslip angle needs to be constrained to zero value. Hence, the angle of incidence of initial trim point should be equal to that of the final flight condition. In addition, the initial trim point should have a zero sideslip value. Such an initial trim point can again be obtained from the results of Fig. 4. Point 2 of Fig. 4 can be noted to correspond to the desired angle of attack and zero sideslip condition and is therefore chosen as the initial operating point. The state vector and control inputs for this initial flight condition, as available from the solution of Eqs. (1) and (12) using EBA method, are

$$[V, \alpha, \beta, p, q, r, \phi, \theta]_{\text{i}} = [280.5, 0.17453, 0, 0, 0, 0, 0, 0.17453] \tag{21}$$

$$\eta = 0.364, \qquad \delta_e = -0.01791, \qquad \delta_a = 0, \qquad \delta_r = 0 \tag{22}$$

C. Spin Recovery Maneuver

The objective of this maneuver is to recover the aircraft from a developed spin condition to a low-angle-of-attack, steady, level, symmetric flight condition. A detailed standard bifurcation analysis of the spin behavior of F-18/HARV has been performed earlier by Raghavendra et al. [25]. The aircraft is shown to enter into a flat oscillatory spin state at an angle of attack exceeding a value of around 72 deg. The spin states have been computed here employing the same procedure as discussed in [25].

The spin states and control deflections computed from bifurcation analysis of Eqs. (1) are

$$\mathbf{x}_{\mathrm{i}} = [207.58, 1.2375, 0.0382, -0.6163, 0.1784, -1.4645, -0.0248, -0.3194]^T \quad (23)$$

$$\eta = 0.36, \qquad \delta_e = -0.44, \qquad \delta_a = 0, \qquad \delta_r = 0 \quad (24)$$

Floquet multipliers for the corresponding periodic solution are also computed by AUTO software as part of the bifurcation analysis procedure. Values of Floquet multipliers for the spin solution (23) are given as $[1.0, 0.8 \pm 0.2103\mathrm{i}, -0.228 \pm 0.592\mathrm{i}, 0.453, 0.187 \pm 0.189\mathrm{i}]$.

It is desired to recover the aircraft to a steady, level, symmetric trim point at an angle of attack of 0.3 rad. Such an operating point can be obtained from the results of Fig. 4. Point 3 of Fig. 4 can be noted to satisfy the required constraints and so is chosen. The state vector and control inputs for this final trim point available from the solution of Eqs. (1) and (12) using EBA are

$$\mathbf{x}_{\mathrm{f}} = [230.2, 0.3, 0, 0, 0, 0, 0, 0.3]^T \quad (25)$$

$$\eta = 0.5445, \qquad \delta_e = -0.0522, \qquad \delta_a = 0, \qquad \delta_r = 0 \quad (26)$$

Spin recovery was also attempted successfully to an angle of attack of 0.5 rad. The results for this case are similar to that shown here for an angle of attack of 0.3 rad, and are therefore not presented.

III. Sliding Mode Control Formulation

SMC is a robust control technique and has been extensively discussed in various references [37–39]. The design procedure for SMC essentially involves two steps. In the first step, a switching surface with desirable properties like stability or tracking is constructed. In the second step, a discontinuous control law that makes the switching surface both attractive and finite time reachable is derived. The transient dynamics in SMC, therefore, evolves in two modes: reaching mode and sliding mode. In reaching mode, the plant's state trajectory shifts from a point in the domain of attraction of the switching surface to a point lying on the switching surface. Once the plant's trajectory intercepts the switching surface, it can not move away from the surface and asymptotically tends to the desired equilibrium point located at the origin of the switching surface; this phase is referred to as the sliding mode. Sliding mode-based control laws are inherently discontinuous and hence result in control chattering. However, the chattering phenomenon can be alleviated to a great extent by continuous approximation of the discontinuous control functions [38] or by using the power rate reaching law method [40].

To design for sliding mode control law, consider an uncertain, nonlinear multi-input/multi-output system in control affine form

$$\dot{\mathbf{x}} = \mathbf{f}(\mathbf{x}) + \Delta\mathbf{f}(\mathbf{x}) + (\mathbf{B}(\mathbf{x}) + \Delta\mathbf{B}(\mathbf{x}))\mathbf{u} \qquad \mathbf{y} = \mathbf{h}(\mathbf{x}) \quad (27)$$

In Eq. (27), $\mathbf{x} = [V, \alpha, \beta, p, q, r, \mu, \gamma]^T \in X \subset \Re^8$ represents the state vector, $\mathbf{u} = [\delta_e, \delta_a, \delta_r]^T \in U \subset \Re^3$ is the control input vector, and $\mathbf{y} = \mathbf{h}(\mathbf{x})$ denotes the output vector for the system. Engine throttle is varied in an open-loop fashion here and is therefore not included in the control vector. The initial and final values of throttle parameter η for open-loop control are already available from the bifurcation analysis results. Vector $\Delta\mathbf{f}(\mathbf{x})$ and matrix $\Delta\mathbf{B}(\mathbf{x})$ represent bounded uncertainties in $\mathbf{f}(\mathbf{x})$ and the control input matrix $\mathbf{B}(\mathbf{x})$, respectively. It is further assumed that all the states of the system represented by Eq. (27) are available for feedback to synthesize the SMC control law.

Assume that for any integer $j \in [0, \gamma_i - 2]$

$$(\nabla(L_{\mathbf{f}}^j h_i(\mathbf{x})))\Delta\mathbf{B}(\mathbf{x}) = 0 \quad (28a)$$

$$(\nabla(L_{\mathbf{f}}^j h_i(\mathbf{x})))\Delta\mathbf{f}(\mathbf{x}) = 0 \quad (28b)$$

Hence, the relative degree of output vector $\mathbf{y}$ can be defined as

$$\begin{aligned} y_i^{(1)} &= L_{\mathbf{f}} h_i(\mathbf{x}) \\ y_i^{(2)} &= L_{\mathbf{f}}^2 h_i(\mathbf{x}) \\ &\vdots \\ y_i^{(\gamma_i)} &= L_{\mathbf{f}}^{\gamma_i} h_i(\mathbf{x}) + L_{\Delta\mathbf{f}} L_{\mathbf{f}}^{\gamma_i - 1} h_i(\mathbf{x}) + \nabla(L_{\mathbf{f}}^{\gamma_i - 1} h_i(\mathbf{x}))(\mathbf{B}(\mathbf{x}) \\ &\quad + \Delta\mathbf{B}(\mathbf{x}))\mathbf{u} \end{aligned} \quad (29)$$

where y_i refers to the ith component of output vector, and $L_{\mathbf{f}} h_i(\mathbf{x})$ denotes the first Lie derivative of output function h_i with respect to the vector function $\mathbf{f}(\mathbf{x})$.

Define the following vectors

$$\begin{aligned} \mathbf{f}^{\mathrm{nom}} &= [L_{\mathbf{f}}^{\gamma_1} h_1(\mathbf{x}), L_{\mathbf{f}}^{\gamma_2} h_2(\mathbf{x}), L_{\mathbf{f}}^{\gamma_3} h_3(\mathbf{x})]^T \\ \Delta\mathbf{f}^{\mathrm{nom}} &= [L_{\Delta\mathbf{f}} L_{\mathbf{f}}^{\gamma_1 - 1} h_1(\mathbf{x}), L_{\Delta\mathbf{f}} L_{\mathbf{f}}^{\gamma_2 - 1} h_2(\mathbf{x}), L_{\Delta\mathbf{f}} L_{\mathbf{f}}^{\gamma_3 - 1} h_3(\mathbf{x})]^T \end{aligned} \quad (30)$$

Again, define the matrices

$$\begin{aligned} \mathbf{B}^{\mathrm{nom}} &= \begin{bmatrix} \nabla(L_{\mathbf{f}}^{\gamma_1 - 1} h_1(\mathbf{x})) \\ \nabla(L_{\mathbf{f}}^{\gamma_2 - 1} h_2(\mathbf{x})) \\ \nabla(L_{\mathbf{f}}^{\gamma_3 - 1} h_3(\mathbf{x})) \end{bmatrix} \mathbf{B}(\mathbf{x}) \\ \Delta\mathbf{B}^{\mathrm{nom}} &= \begin{bmatrix} \nabla(L_{\mathbf{f}}^{\gamma_1 - 1} h_1(\mathbf{x})) \\ \nabla(L_{\mathbf{f}}^{\gamma_2 - 1} h_2(\mathbf{x})) \\ \nabla(L_{\mathbf{f}}^{\gamma_3 - 1} h_3(\mathbf{x})) \end{bmatrix} \Delta\mathbf{B}(\mathbf{x}) \end{aligned} \quad (31)$$

The matrix $\mathbf{B}^{\mathrm{nom}}$ is assumed to be nonsingular so that the nominal system can be decoupled using state feedback [28,41] and hence can be input–output linearized [38].

Let the total relative degree $\gamma = (\gamma_1 + \gamma_2 + \gamma_3) < n$, where n is the order of the given system. Under such conditions, the uncertain system (27) can be transformed into a normal form using the state vector $\boldsymbol{\xi} = [y_1, y_1^{(1)}, \ldots, y_1^{(\gamma_1 - 1)}, \ldots, y_3, y_3^{(1)}, \ldots, y_3^{(\gamma_3 - 1)}]^T$ and $\varphi = \varphi(\mathbf{x})$ as

$$\begin{aligned} \dot{\boldsymbol{\xi}} &= \mathbf{C}\boldsymbol{\xi} + \mathbf{D}(\mathbf{f}^{\mathrm{nom}} + \Delta\mathbf{f}^{\mathrm{nom}} + (\mathbf{B}^{\mathrm{nom}} + \Delta\mathbf{B}^{\mathrm{nom}})\mathbf{u}) \\ \dot{\varphi} &= \mathbf{f}(\varphi, \boldsymbol{\xi}) \end{aligned} \quad (32)$$

where $\mathbf{f}(\varphi, \boldsymbol{\xi})$ represents the internal dynamics of the system. For the controller design to be feasible, the internal dynamics of the system should be stable [38]. The internal dynamics for the maneuvers simulated in this work is influenced by open-loop throttle control: the magnitude of required throttle for final steady state being directly available from the bifurcation analysis results.

Following the notations of Singh [28], the matrices C and D can be conveniently expressed as

$$\mathbf{C} = \mathrm{diag}[C_i]; \qquad i = 1, \ldots, 3 \qquad C_i = \begin{bmatrix} 0 & 1 & 0 \ldots 0 \\ 0 & 0 & 1 \ldots 0 \\ 0 & 0 & 0 \ldots 1 \\ 0 & 0 & 0 \ldots 0 \end{bmatrix} \quad (33)$$

The matrix D can be expressed as

$$\mathbf{D} = \mathrm{diag}[C_i]; \qquad i = 1, \ldots, 3 \qquad D_i = [0, 0, 0, \ldots, 1]^{\mathrm{T}} \quad (34)$$

where $\mathrm{diag}(*)$ represents a diagonal matrix. Matrix C_i is of dimension $\gamma_i \times \gamma_i$, and D_i is of dimension $\gamma_i \times 1$.

Let the reference trajectory $\mathbf{R}$ be

$$\mathbf{R} = [y_{1r}, y_{1r}^{(1)}, \ldots, y_{1r}^{(\gamma_1 - 1)}, \ldots, y_{3r}, y_{3r}^{(1)}, \ldots, y_{3r}^{(\gamma_3 - 1)}]^T \quad (35)$$

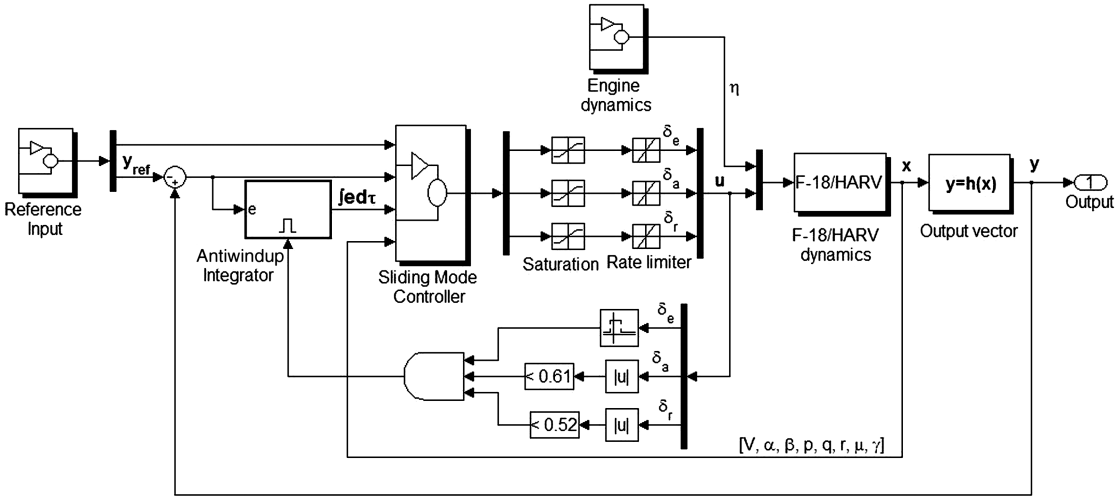

Fig. 7 Simulink block diagram for the closed-loop system with SMC controller.

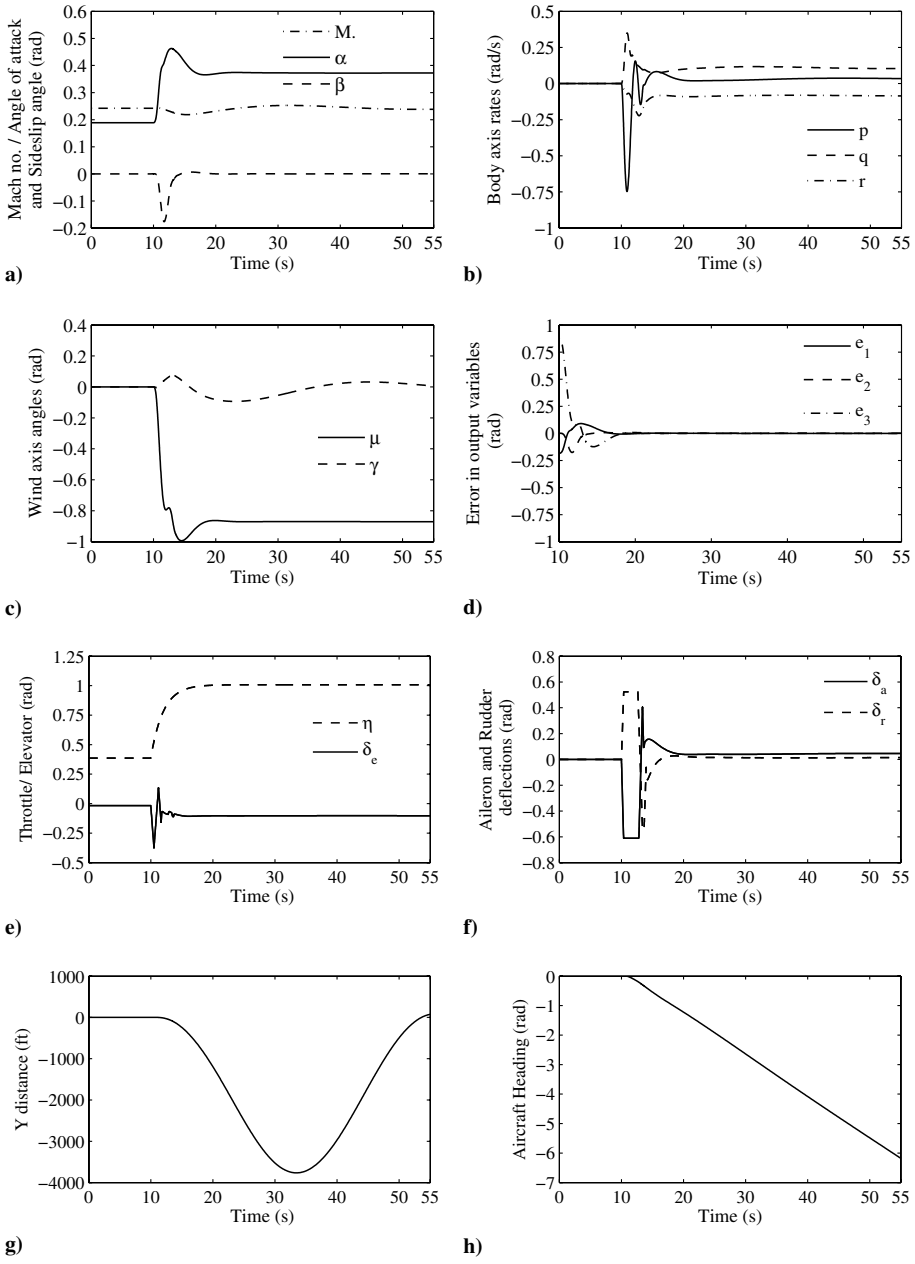

Fig. 8 Time history of aircraft parameters for minimum-radius turn maneuver using SMC with +25% uncertainty in aerodynamic derivatives.

Define a vector of error variables

$$\mathbf{e} = \boldsymbol{\xi} - \mathbf{R} \qquad \mathbf{e} = [e_1, e_1^{(1)}, \ldots, e_1^{(\gamma_1-1)}, \ldots, e_3, e_3^{(1)}, \ldots, e_3^{(\gamma_3-1)}]^T \tag{36}$$

Hence, Eq. (32) can be expressed in terms of error variables as

$$\dot{\mathbf{e}} = \dot{\boldsymbol{\xi}} - \dot{\mathbf{R}} \qquad \dot{\varphi} = \mathbf{f}(\varphi, \boldsymbol{\xi}) \tag{37}$$

Choose a sliding surface

$$\mathbf{s} = 0 \tag{38}$$

where $\mathbf{s} = [s_1, s_2, s_3]^T$.

Here, we choose the switching variable s_i to be of the form

$$s_i = \left[k_{i0} \int_0^t e_i \mathrm{d}\tau + k_{i1} e_i + k_{i2} e_i^{(1)}, \ldots, k_{i(\gamma_i-1)} e_i^{(\gamma_i-2)} + e_i^{(\gamma_i-1)} \right] \tag{39}$$

where the coefficients k_{ij} $(i = 1, ..., 3$ and $j = 0, ..., \gamma_i - 1)$ are selected such that the corresponding polynomial formed by the coefficients of s_i is Hurwitz.

Differentiating Eq. (39) with respect to time, for $i = 1, ..., 3$, gives

$$\dot{\mathbf{s}} = \mathbf{P}\mathbf{e} + \mathbf{Q}\dot{\mathbf{e}} \tag{40}$$

where

$$\mathbf{P} = \mathrm{diag}[P_i]; \qquad i = 1, \ldots, 3 \qquad P_i = [k_{i0}, k_{i1}, \ldots, k_{i\gamma_i-1}] \tag{41}$$

The matrix $\mathbf{Q}$ is given as

$$\mathbf{Q} = \mathrm{diag}[Q_i] \qquad i = 1, \ldots, 3 \qquad Q_i = [0, 0, \ldots, 1] \in \Re^{\gamma_i} \tag{42}$$

where matrices $\mathbf{P}$ and $\mathbf{Q}$ are of dimension $3 \times (\gamma_1 + \gamma_2 + \gamma_3)$.

Substituting Eqs. (36) and (37) in Eq. (40)

$$\dot{\mathbf{s}} = \mathbf{P}\mathbf{e} + \mathbf{f}^{\mathrm{nom}} + \Delta\mathbf{f}^{\mathrm{nom}} + (\mathbf{B}^{\mathrm{nom}} + \Delta\mathbf{B}^{\mathrm{nom}})\mathbf{u} - \mathbf{Q}\dot{\mathbf{R}} \tag{43}$$

since $\mathbf{QC} = [\mathbf{0}]$ and $\mathbf{QD} = \mathbf{I}$; $\mathbf{I}$ being an identity matrix.

Choose the control input vector as

$$\mathbf{u} = (\mathbf{B}^{\mathrm{nom}})^{-1}[-\mathbf{f}^{\mathrm{nom}} - \mathbf{P}\mathbf{e} + \mathbf{Q}\dot{\mathbf{R}} - \mathbf{K}(\mathbf{s})\mathrm{sgn}(\mathbf{s})] \tag{44}$$

Substituting Eq. (44) in Eq. (43)

$$\dot{\mathbf{s}} = -(\mathbf{I} + (\Delta\mathbf{B}^{\mathrm{nom}})(\mathbf{B}^{\mathrm{nom}})^{-1})\mathbf{K}(\mathbf{s})\mathrm{sgn}(\mathbf{s}) + \Delta\mathbf{f}^{\mathrm{nom}} + (\Delta\mathbf{B}^{\mathrm{nom}})(\mathbf{B}^{\mathrm{nom}})^{-1}[-\mathbf{f}^{\mathrm{nom}} - \mathbf{P}\mathbf{e} + \mathbf{Q}\dot{\mathbf{R}}] \tag{45}$$

where $\mathrm{sgn}(\mathbf{s}) = [\mathrm{sgn}(s_1), \mathrm{sgn}(s_2), \mathrm{sgn}(s_3)]^{\mathrm{T}}$.

The gain matrix $\mathbf{K}(\mathbf{s})$ is chosen as a sum of power law [40] and a constant term

$$\mathbf{K}(\mathbf{s}) = \frac{\mathrm{diag}(\varepsilon|s_i|^{\alpha} + b)}{(1 - a)} \tag{46}$$

where $\varepsilon > 0$ and $\alpha \in (0, 1)$. The constants a and b are positive real numbers, and their values are determined based on the bounds on uncertainties in the model as given in Eqs. (49) and (50).

To prove that the switching surface defined in Eqs. (38) and (39) is attractive and finite time reachable, consider a Lyapunov function candidate

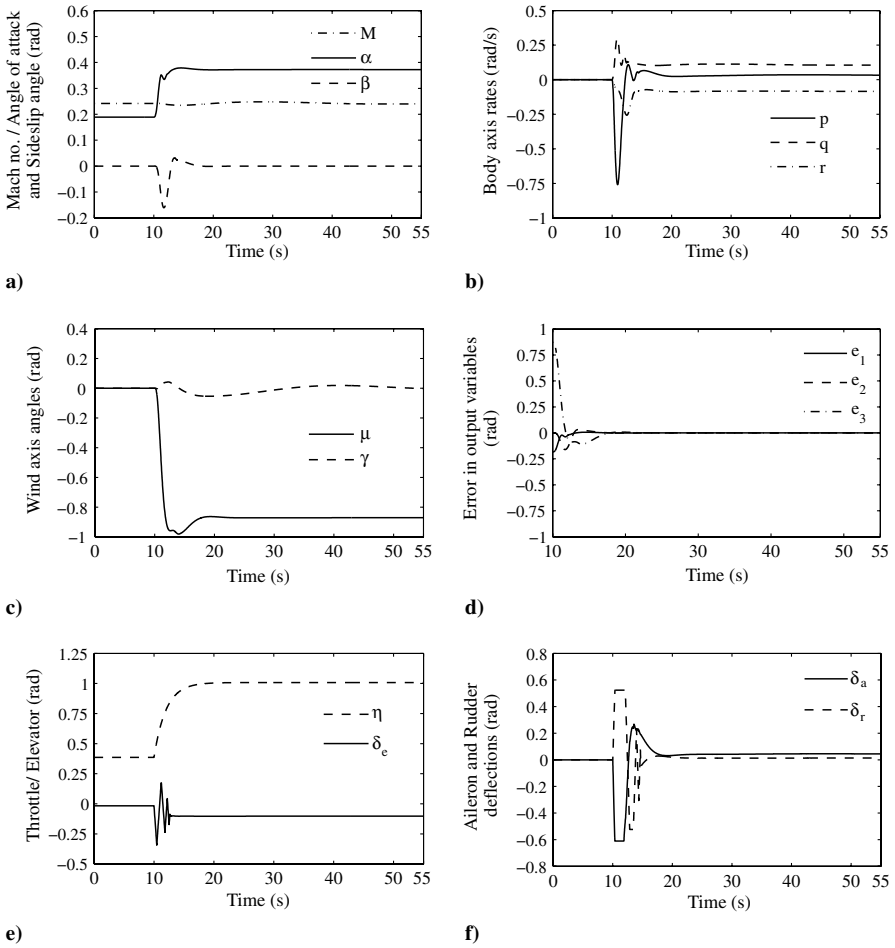

Fig. 9 Time history of aircraft parameters for minimum-radius turn maneuver using SMC with −25% uncertainty in aerodynamic derivatives.

$$V = \frac{1}{2}\mathbf{s}^T\mathbf{s} > 0, \quad \forall\ \mathbf{s} \neq 0 \tag{47}$$

Taking the time derivative of Eq. (47)

$$\dot{V} = \mathbf{s}^T[-(\mathbf{I} + (\Delta\mathbf{B}^{\text{nom}})(\mathbf{B}^{\text{nom}})^{-1})\mathbf{K}(\mathbf{s})\text{sgn}(\mathbf{s}) + \Delta\mathbf{f}^{\text{nom}} + (\Delta\mathbf{B}^{\text{nom}})(\mathbf{B}^{\text{nom}})^{-1}\{-\mathbf{f}^{\text{nom}} - \mathbf{Pe} + Q\dot{\mathbf{R}}\}] \tag{48}$$

Now, consider the following bounds on uncertain terms

$$\| (\Delta\mathbf{B}^{\text{nom}})(\mathbf{B}^{\text{nom}})^{-1}) \|_\infty \leq a < \frac{1}{3} \tag{49}$$

$$\| \Delta\mathbf{f}^{\text{nom}} + (\Delta\mathbf{B}^{\text{nom}})(\mathbf{B}^{\text{nom}})^{-1}(-\mathbf{f}^{\text{nom}} - \mathbf{Pe} + \mathbf{Q}\dot{\mathbf{R}}) \|_\infty \leq b \tag{50}$$

where the uncertainty bounds in Eqs. (49) and (50) are expressed in a form similar to that presented in [23].

Substituting Eqs. (46), (49), and (50) in Eq. (48) and rearranging,

$$\dot{V} \leq -\frac{\varepsilon}{(1-a)}\sum_{i=1}^{3}|s_i|^{\alpha+1} + \frac{a\varepsilon}{(1-a)}\sum_{i=1}^{3}|s_i|\sum_{i=1}^{3}|s_i|^{\alpha} \tag{51}$$

Using Chebyshev's sum inequality, Eq. (51) can be expressed as

$$\dot{V} \leq -\frac{\varepsilon(1-3a)}{(1-a)}\sum_{i=1}^{3}|s_i|^{\alpha+1} < 0, \quad \forall\ \mathbf{s} \neq 0 \tag{52}$$

Hence, from Eqs. (47) and (52), it can be inferred that the selected switching surface is both attractive and finite time reachable.

A. Control of α, β, and μ

In an aircraft control problem, aerodynamic control forces can generally be omitted in comparison to the control moments [28,42]. We neglect these control forces for the purpose of controller design here; this has the equivalent effect of removing the nonminimum phase plant behavior, which can destabilize the internal dynamics of

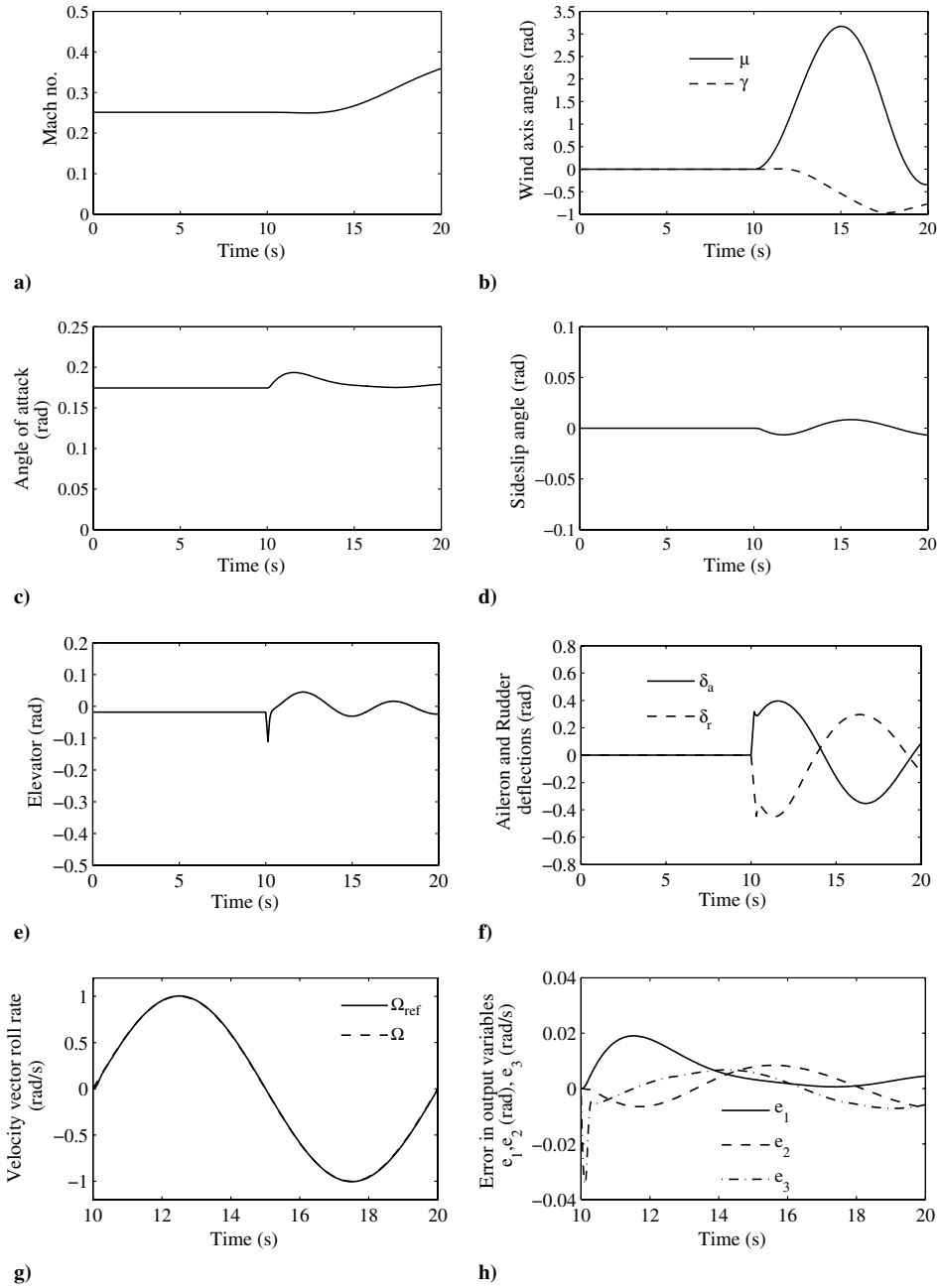

Fig. 10 Time history of aircraft parameters for VVR maneuver using SMC with +25% uncertainty in aerodynamic derivatives.

the closed-loop system. The assumption (28a) is therefore satisfied. We further assume that the uncertain term (28b) is small enough that its influence on lower order derivatives of y_i can be ignored.

The output vector $\mathbf{y} = [\alpha, \beta, \mu]^T$ and the relative degrees are $\gamma_1 = 2$, $\gamma_2 = 2$, and $\gamma_3 = 2$.

The vector

$$\mathbf{f}^{\text{nom}} = [L_{\mathbf{f}}^2\alpha, L_{\mathbf{f}}^2\beta, L_{\mathbf{f}}^2\mu]^T \tag{53}$$

and the matrix

$$\mathbf{B}^{\text{nom}} = \begin{bmatrix} \nabla(L_{\mathbf{f}}\alpha) \\ \nabla(L_{\mathbf{f}}\beta) \\ \nabla(L_{\mathbf{f}}\mu) \end{bmatrix} \mathbf{B}(\mathbf{x}) \tag{54}$$

Choosing the reference trajectory $\mathbf{R}$ as

$$\mathbf{R} = [\alpha_r, \dot{\alpha}_r, \beta_r, \dot{\beta}_r, \mu_r, \dot{\mu}_r]^T \tag{55}$$

The vector of error variables can be expressed as

$$\mathbf{e} = \boldsymbol{\xi} - \mathbf{R} \Rightarrow \mathbf{e} = [\alpha - \alpha_r, \dot{\alpha} - \dot{\alpha_r}, \beta - \beta_r, \dot{\beta} - \dot{\beta_r}, \mu - \mu_r, \dot{\mu} - \dot{\mu_r}]^T \tag{56}$$

The switching variable $\mathbf{s}$ is of the form

$$\mathbf{s} = \begin{bmatrix} k_{10}\int_0^t e_1 d\tau + k_{11}e_1 + \dot{e_1} \\ k_{20}\int_0^t e_2 d\tau + k_{21}e_2 + \dot{e_2} \\ k_{30}\int_0^t e_3 d\tau + k_{31}e_3 + \dot{e_3} \end{bmatrix} \tag{57}$$

Thus, matrices $\mathbf{P}$ and $\mathbf{Q}$ defined in Eqs. (41) and (42) are of the form

$$\mathbf{P} = \begin{bmatrix} k_{10} & k_{11} & 0 & 0 & 0 & 0 \\ 0 & 0 & k_{20} & k_{21} & 0 & 0 \\ 0 & 0 & 0 & 0 & k_{30} & k_{31} \end{bmatrix}$$

$$\mathbf{Q} = \begin{bmatrix} 0 & 1 & 0 & 0 & 0 & 0 \\ 0 & 0 & 0 & 1 & 0 & 0 \\ 0 & 0 & 0 & 0 & 0 & 1 \end{bmatrix} \tag{58}$$

Hence, the control law can be evaluated by substituting Eqs. (53–58) in Eq. (44).

B. Control of α, β, and Ω

Here, $\mathbf{y} = [\alpha, \beta, \Omega]^T$ is the output vector for the system. The variable Ω represents the velocity vector roll rate as given by Eq. (18). The simplified expression for Ω is given as

$$\Omega = p\ \cos\alpha\cos\beta + q\ \cos\alpha\sin\beta + r\ \sin\alpha\cos\beta \tag{59}$$

Because aerodynamic control forces are neglected, the relative degree $\gamma_1 = 2$, $\gamma_2 = 2$, and $\gamma_3 = 1$.

The vector

$$\mathbf{f}^{\text{nom}} = [L_{\mathbf{f}}^2\alpha, L_{\mathbf{f}}^2\beta, L_{\mathbf{f}}\Omega]^T \tag{60}$$

and the matrix

$$\mathbf{B}^{\text{nom}} = \begin{bmatrix} \nabla(L_{\mathbf{f}}\alpha) \\ \nabla(L_{\mathbf{f}}\beta) \\ \nabla(\Omega) \end{bmatrix} \mathbf{B}(\mathbf{x}) \tag{61}$$

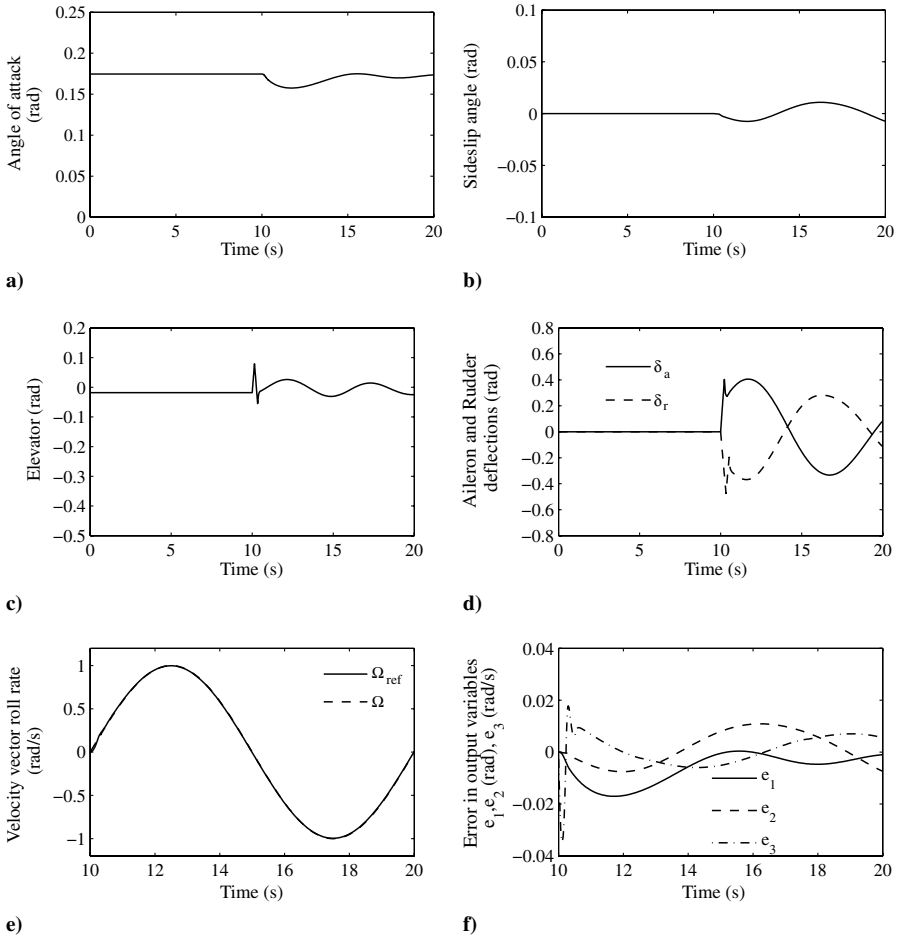

Fig. 11 Time history of aircraft parameters for VVR maneuver using SMC with −25% uncertainty in aerodynamic derivatives.

Let the reference trajectory **R** be

$$\mathbf{R} = [\alpha_r, \dot{\alpha}_r, \beta_r, \dot{\beta}_r, \Omega_r]^T \tag{62}$$

The vector of error variables can then be expressed as

$$\mathbf{e} = \boldsymbol{\xi} - \mathbf{R} \Rightarrow \mathbf{e} = [\alpha - \alpha_r, \dot{\alpha} - \dot{\alpha}_r, \beta - \beta_r, \dot{\beta} - \dot{\beta}_r, \Omega - \Omega_r]^T \tag{63}$$

The switching variable **s** is of the form

$$\mathbf{s} = \begin{bmatrix} k_{10}\int_0^t e_1\,\mathrm{d}\tau + k_{11}e_1 + \dot{e_1} \\ k_{20}\int_0^t e_2\,\mathrm{d}\tau + k_{21}e_2 + \dot{e_2} \\ k_{30}\int_0^t e_3\,\mathrm{d}\tau + e_3 \end{bmatrix} \tag{64}$$

Thus, matrices **P** and **Q** defined in Eqs. (41) and (42) are of the form

$$\mathbf{P} = \begin{bmatrix} k_{10} & k_{11} & 0 & 0 & 0 \\ 0 & 0 & k_{20} & k_{21} & 0 \\ 0 & 0 & 0 & 0 & k_{30} \end{bmatrix} \qquad \mathbf{Q} = \begin{bmatrix} 0 & 1 & 0 & 0 & 0 \\ 0 & 0 & 0 & 1 & 0 \\ 0 & 0 & 0 & 0 & 1 \end{bmatrix} \tag{65}$$

Substitute Eqs. (60–65) in Eq. (44) to evaluate the expression for the sliding mode control law.

IV. Results and Discussion

Closed-loop simulation results for F-18/HARV maneuvers constructed in Sec. II are presented in this section. A complete 6-DOF, nonlinear aircraft model is used for simulating all the maneuvers here. The numerical simulations are performed in MATLAB Simulink environment. ISA sea level conditions are assumed for ambient atmospheric variables, and the effect of density variation due to change in altitude has been neglected for simulation. In the plots shown, velocity has been nondimensionalized to corresponding Mach number using suitable speed of sound, $v_s = 1116$ ft/s. The aerodynamic derivatives used in controller

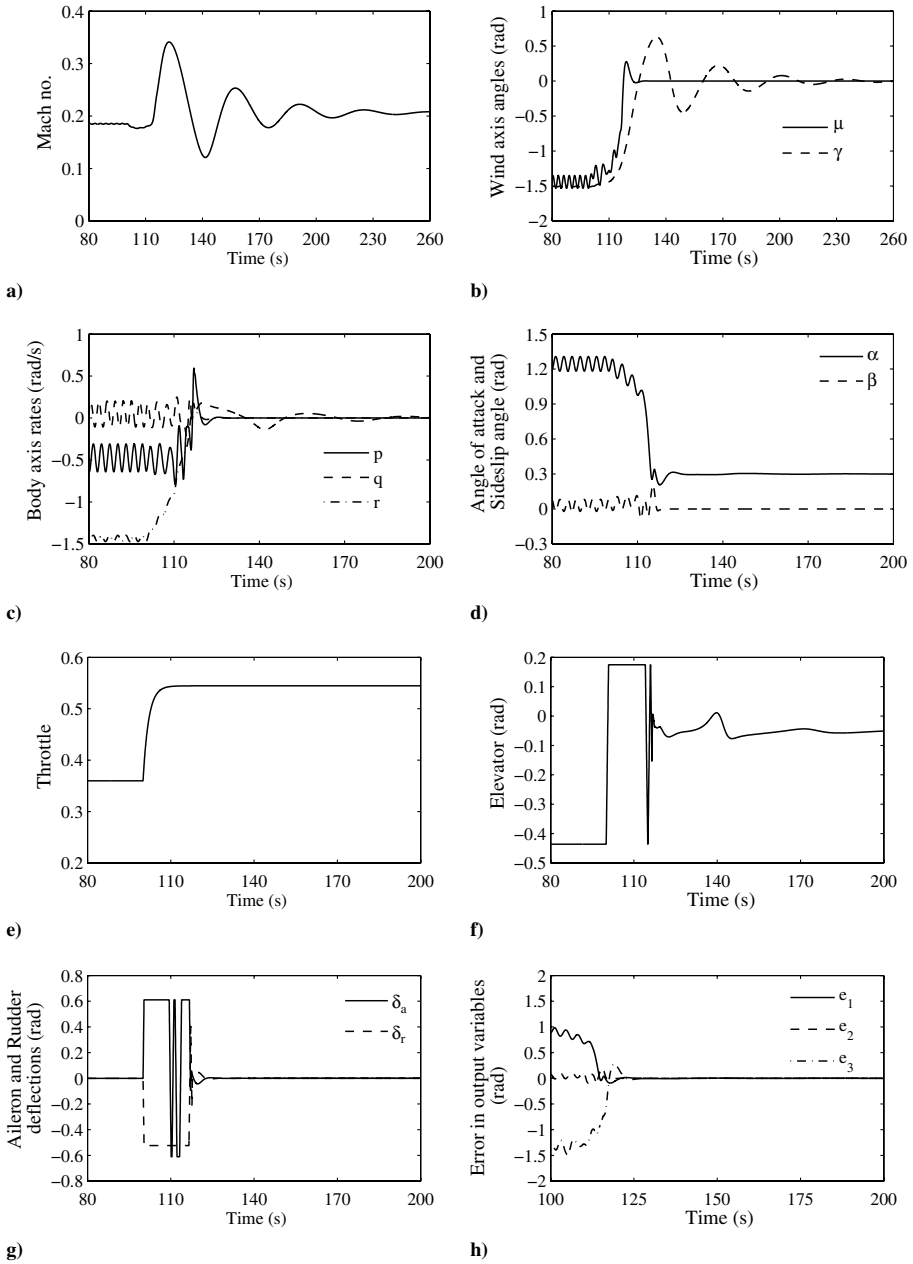

Fig. 12 Time history of aircraft parameters for spin recovery maneuver using SMC with +25% uncertainty in aerodynamic derivatives.

design are uniformly perturbed by ±25% to assess the robustness of the SMC controller designed in the last section. However, the aerodynamic derivatives for the plant model remain unaltered. The constants k_{i0} and k_{i1} $(i = 1, ..., 3)$ in the expression for switching surface (39) are set as 0.6 and 1.0, respectively, and constant α in expression (46) is taken as 0.9. From numerical simulations, it is observed that, by taking a large value of ε in Eq. (46), the b term in the expression for gain matrix $\mathbf{K(s)}$ can be ignored. The parameter ε has been fixed at a numerical value of 10 for all the results presented in this work.

Figure 7 shows the Simulink block diagram for the closed-loop system. A simple antiwindup logic is also included in the closed-loop system to prevent any integral windup. The antiwindup logic is similar to that used with most of the proportional-integral linear controllers; integral action is kept active as long as all the three aerodynamic controls are within their position limits and is switched off whenever any of the three control effectors hits its position limit. Effect of control surfaces' actuator position and rate constraints are also included in the loop for a realistic simulation.

Figures 8 and 9 show the results for a minimum-radius turn maneuver. The aircraft is initially flying in a steady, level, symmetric trim condition for about 10 s. The SMC controller is activated at $t = 10$ s to switch the aircraft into the sustained minimum-radius turn flight condition by specifying the final values of three output variables ($\mathbf{y} = [\alpha, \beta, \mu]^T$) as step commands. It can be noticed from Figs. 8d and 9d that the errors in the output variables (α, β, and μ) reduce to zero in less than 10 s from the start of control action; body axis rates, shown in Figs. 8b and 9b, also settle down to their respective steady-state values within the same time duration. The variation in Mach number and flight path angle γ for +25% uncertain case is found to be slightly higher than that with −25% uncertainty. The radius of turn, from Fig. 8g, can be observed to be around 1900 ft, which is very close to the value predicted from bifurcation analysis results presented in Fig. 3. Time taken to complete the turn can be noted to be around 45 s from Fig. 8h. The Y distance and heading angle variations for the −25% uncertain case are similar to that shown in Figs. 8g and 8h and are therefore not shown. Time histories of SMC generated control inputs are depicted in Figs. 8e, 8f, 9e, and 9f. The initial sense of SMC command inputs can be observed to be such as to provide a left aileron along with a left rudder to maintain a coordinated roll to the left; a simultaneous nose-up elevator input helps in increasing the angle of attack to the required value. Engine

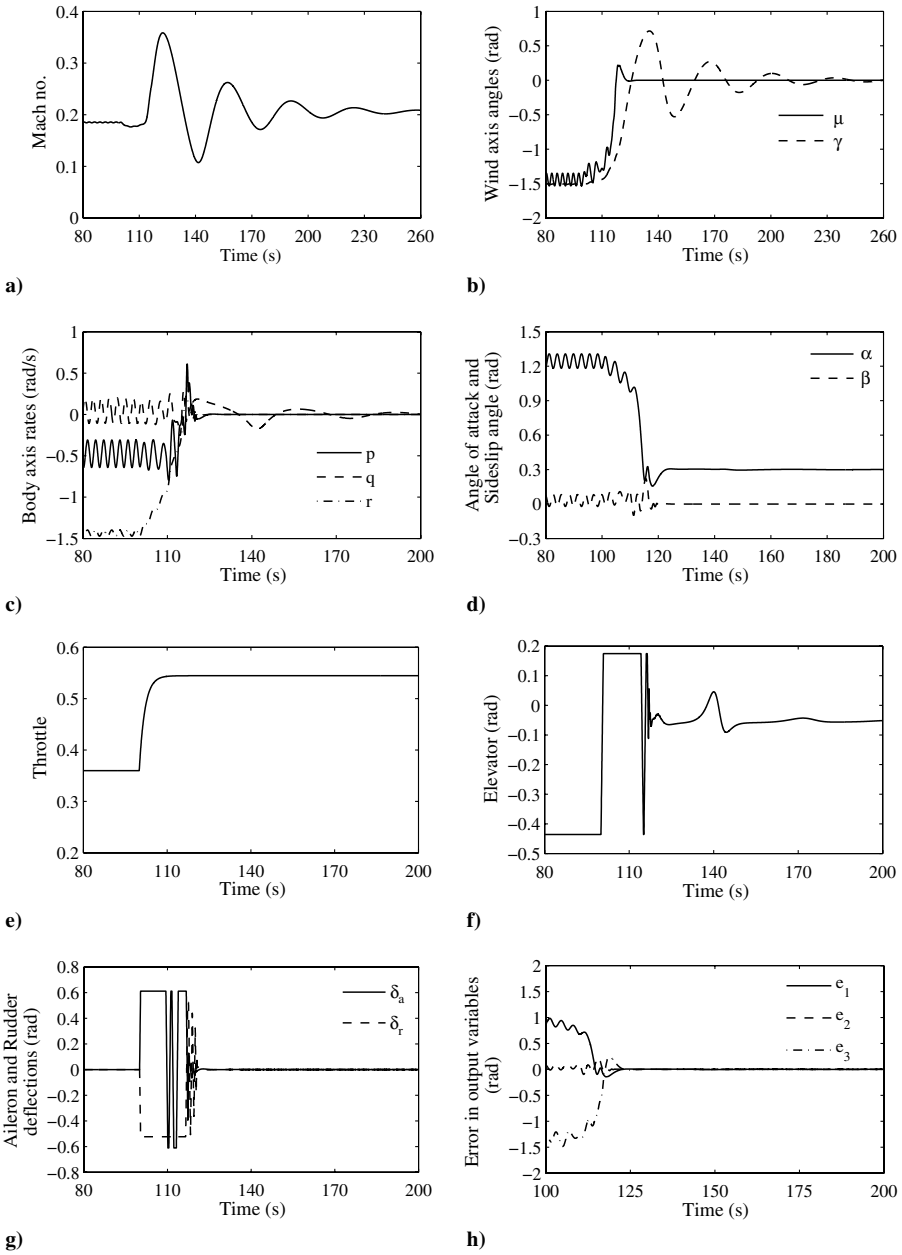

Fig. 13 Time history of aircraft parameters for spin recovery maneuver using SMC with −25% uncertainty in aerodynamic derivatives.

throttle response, shown in Figs. 8e and 9e, is controlled in an open-loop manner with a simple lag of time constant 2 s: the initial and final values of throttle parameter η being already known from bifurcation analysis results. The control activity for -25% uncertain results can be observed to be higher than for the $+25\%$ uncertain case; this is caused by lower aerodynamic damping and lower aerodynamic control effectiveness in the -25% uncertain case because the aerodynamic derivatives are assumed to be considerably lower than their nominal values.

VVR maneuver results are shown in Figs. 10 and 11. The aircraft is flying in an initial steady, level, symmetric flight condition for about 10 s. The SMC controller is then commanded at $t = 10$ s to track the sinusoidal velocity vector roll rate command Ω_{ref}, while holding angle of attack at initial value and regulating sideslip to zero. It can be seen from Figs. 10g and 11e that the reference velocity vector roll rate Ω_{ref} is tracked quite accurately. The fluctuations observed in the three output variables ($\mathbf{y} = [\alpha, \beta, \Omega]^T$) are quite small, as is evident from the error plots of Figs. 10h and 11f and also from Figs. 10c, 10d, 11a, and 11b. Time history of aircraft flight path angle γ during the roll maneuver is presented in Fig. 10b, which shows the aircraft in a descending flight path during the roll maneuver. Variations in γ and μ for the -25% uncertain case are similar to that shown in Fig. 10b and are therefore not presented. Time histories of SMC control commands are shown in Figs. 10e, 10f, 11c, and 11d: No saturation in any of the control effectors is observed during the roll maneuver from these plots. Thrust is held constant at the initial level flight condition value and so is not depicted. A notable rise in speed, though, can be observed from Fig. 10a as a result of aircraft entering into a descent. Mach number plot for results with -25% uncertainty is identical to the plot of Fig. 10a and is therefore not shown.

Results for the spin recovery maneuver are presented in Figs. 12 and 13. Initial conditions for spin are specified and an open-loop simulation is done for starting 100 s to account for any deviation in prescribing spin states. Control action is initiated at $t = 100$ s to recover the aircraft out of spin condition by passing the final values of the three output variables ($\mathbf{y} = [\alpha, \beta, \mu]^T$) as step inputs to the controller. It can be observed from the plots of Figs. 12h and 13h that the three output variables (α, β, and μ) stabilize to their respective final steady-state values within 25 s of the initiation of control action. Body axis roll and yaw rates shown in Figs. 12c and 13c also reduce to zero within the same time span; the pitch rate, however, takes a longer time to stabilize because of aircraft entering into a lightly damped phugoid mode. Engine throttle, shown in Figs. 12e and 13e, is controlled in an open-loop manner with a simple lag of time constant 2 s. Time histories of command inputs from SMC controller are shown in Figs. 12f, 12g, 13f, and 13g. The sense of initial control commands from the controller is found to be such as to deflect the rudder to the right, which helps in arresting the large left yaw rate existing in spin condition; a simultaneous nose-down elevator command assists in lowering the angle of attack to pull the aircraft out of spin condition. The control activity for aileron and rudder control command inputs for the -25% uncertain case can be seen to be more severe than for results with $+25\%$ uncertainty; this happens due to reduced aerodynamic damping and lesser aerodynamic controls' power for the -25% uncertain case because stability and control derivatives are assumed to be lower than their nominal values.

V. Conclusions

This work demonstrates an effective implementation of the two well-known techniques of analysis and control design of nonlinear systems for efficiently designing aircraft maneuvers. Bifurcation analysis is a powerful methodology to examine global dynamics of nonlinear systems, and sliding mode control (SMC) is a robust control technique for controlling nonlinear plant models. The two approaches have been used in conjunction to design and simulate maneuvers for a nonlinear aircraft model. A constrained bifurcation analysis is first carried out to obtain bifurcation plots for the model under specified maneuver constraints. The bifurcation map, thus obtained, is used as a guideline to construct the desired maneuvers by identifying the initial and final steady states of the maneuver that provide the necessary controlled variables to be used as reference inputs for the SMC controller to simulate the maneuver. Closed-loop simulation results of three different maneuvers highlight the usefulness of this combined approach. The proposed strategy can also be extended to design various other complicated flight maneuvers that may require specifications of multiple set of trim points, instead of a single set of trim points used in this work.

Appendix: Equations of Motion and Aircraft Data

The rigid body aircraft flight dynamic equations [2]

$$\dot{V} = \frac{1}{m}\left[T_m\eta\cos\alpha\cos\beta - \frac{1}{2}\rho V^2 S C_D(\alpha, q, \delta_e) - mg\sin\gamma\right]$$

$$\dot{\alpha} = q - \frac{1}{\cos\beta}\left[(p\cos\alpha + r\sin\alpha)\sin\beta + \frac{1}{mV}\left\{T_m\eta\sin\alpha + \frac{1}{2}\rho V^2 S C_L(\alpha, q, \delta_e) - mg\cos\mu\cos\gamma\right\}\right]$$

$$\dot{\beta} = \frac{1}{mV}\left[-T_m\eta\cos\alpha\sin\beta + \frac{1}{2}\rho V^2 S C_Y(\alpha, \beta, p, r, \delta_e, \delta_a, \delta_r) + mg\sin\mu\cos\gamma\right] + (p\sin\alpha - r\cos\alpha)$$

$$\dot{p} = \frac{I_y - I_z}{I_x}qr + \frac{1}{2I_x}\rho V^2 S b C_l(\alpha, \beta, p, r, \delta_e, \delta_a, \delta_r)$$

$$\dot{q} = \frac{I_z - I_x}{I_y}pr + \frac{1}{2I_y}\rho V^2 S c C_m(\alpha, q, \delta_e)$$

$$\dot{r} = \frac{I_x - I_y}{I_z}pq + \frac{1}{2I_z}\rho V^2 S b C_n(\alpha, \beta, p, r, \delta_e, \delta_a, \delta_r)$$

$$\dot{\phi} = p + q\sin\phi\tan\theta + r\cos\phi\tan\theta$$

$$\dot{\theta} = q\cos\phi - r\sin\phi$$

$$\dot{\psi} = \frac{q\sin\phi + r\cos\phi}{\cos\theta}$$

$$\dot{X} = V\cos\gamma\cos\chi; \qquad \dot{Y} = V\cos\gamma\sin\chi; \qquad \dot{Z} = -V\sin\gamma$$

The dynamics of μ, γ, and χ are given by the following equations [21]:

$$\dot{\mu} = \sec\beta(p\cos\alpha + r\sin\alpha) + \frac{1}{mV}\left[\frac{1}{2}\rho V^2 S C_L(\alpha, q, \delta_e)\{\tan\beta + \sin\mu\tan\gamma\} - mg\cos\mu\cos\gamma\tan\beta + T_m\eta\{\sin\alpha\tan\beta + \sin\alpha\sin\mu\tan\gamma - \cos\alpha\sin\beta\cos\mu\tan\gamma\} + \frac{1}{2}\rho V^2 S C_Y(\alpha, \beta, p, r, \delta_e, \delta_a, \delta_r)\cos\mu\tan\gamma\right]$$

$$\dot{\gamma} = \frac{1}{mV}\left[T_m\eta\{\sin\alpha\cos\mu + \cos\alpha\sin\beta\sin\mu\} + \frac{1}{2}\rho V^2 S C_L(\alpha, q, \delta_e)\cos\mu - mg\cos\gamma - \frac{1}{2}\rho V^2 S C_Y(\alpha, \beta, p, r, \delta_e, \delta_a, \delta_r)\sin\mu\right]$$

$$\dot{\chi} = \frac{1}{mV\cos\gamma}\left[T_m\eta\{\sin\alpha\sin\mu - \cos\alpha\sin\beta\cos\mu\} + \frac{1}{2}\rho V^2 S C_L(\alpha, q, \delta_e)\sin\mu + \frac{1}{2}\rho V^2 S C_Y(\alpha, \beta, p, r, \delta_e, \delta_a, \delta_r)\cos\mu\right]$$

Wind-axis Euler angles μ, γ and body axis Euler angles ϕ, θ, and ψ are also related by the following kinematic relations [2]:

$$\sin\gamma = \cos\alpha\cos\beta\sin\theta - \sin\beta\sin\phi\cos\theta - \sin\alpha\cos\beta\cos\phi\cos\theta$$

$$\sin\mu\cos\gamma = \cos\alpha\sin\beta\sin\theta + \cos\beta\sin\phi\cos\theta - \sin\alpha\sin\beta\cos\phi\cos\theta$$

$$\cos\mu\cos\gamma = \sin\theta\sin\alpha + \cos\alpha\cos\phi\cos\theta$$

Table A1 F-18/HARV data

Parameter	Numerical value
Wingspan, b	37.42 ft
Mean aerodynamic chord, c	11.52 ft
Acceleration due to gravity, g	32 ft/s^2
Roll inertia, I_x	22, 789 slug $\cdot$ ft^2
Pitch inertia, I_y	176, 809 slug $\cdot$ ft^2
Yaw inertia, I_z	191, 744 slug $\cdot$ ft^2
Aircraft mass, m	1128.09 slug
Wing area, S	400 ft^2
Maximum available thrust, T_m	16,000 lb
Density of air, ρ	0.00238 slug/ft^3
Speed of sound, v_s	1116 ft/s

Table A2 Actuator constraints

Control surface	Position limit, deg	Rate limit, deg /s
Elevator, δ_e	$(-25, 10)$	$\pm$ 40
Aileron, δ_a	$(-35, 35)$	$\pm$ 100
Rudder, δ_r	$(-30, 30)$	$\pm$ 82

Acknowledgments

Financial support received for this work from the Aeronautics Research and Development Board, Government of India, is gratefully acknowledged. The authors wish to thank Arun D. Mahindrakar of the Electrical Engineering Department of Indian Institute of Technology–Madras for useful discussions and suggestions on sliding mode control.

References

[1] Schneider, G. L., and Watt, G. W., "Minimum-Time Turns Using Vectored Thrust," *Journal of Guidance, Control, and Dynamics*, Vol. 12, No. 6, 1989, pp. 777–782. doi:10.2514/3.20481

[2] Fan, Y., Lutze, F. H., and Cliff, E. M., "Time-Optimal Lateral Maneuvers of an Aircraft," *Journal of Guidance, Control, and Dynamics*, Vol. 18, No. 5, 1995, pp. 1106–1112. doi:10.2514/3.21511

[3] Komduur, H. J., and Visser, H. G., "Optimization of Vertical Plane Cobralike Pitch Reversal Maneuvers," *Journal of Guidance, Control, and Dynamics*, Vol. 25, No. 4, 2002, pp. 693–702. doi:10.2514/2.4936

[4] Shippey, B., and Subbarao, K., "Trajectory Design Using Collocation and Genetic Algorithms: Aircraft Turning Maneuver," in *Proc. 17th IEEE International Conference on Control Applications Part of 2008 IEEE Multi-conference on Systems and Control*, IEEE Publications, Piscataway, NJ, 2008, pp. 905–911.

[5] Basseta, G., Xua, Y., and Yakimenkob, O. A., "Computing Short-Time Aircraft Maneuvers Using Direct Methods," *Journal of Computer and Systems Sciences International*, Vol. 49, No. 3, 2010, pp. 481–513. doi:10.1134/S1064230710030159

[6] Carroll, J. V., and Mehra, R. K., "Bifurcation Analysis of Nonlinear Aircraft Dynamics," *Journal of Guidance, Control, and Dynamics*, Vol. 5, No. 5, 1982, pp. 529–536. doi:10.2514/3.56198

[7] Goman, M. G., Zagaynov, G. I., and Khramtsovsky, A. V., "Application of Bifurcation Methods to Nonlinear Flight Dynamics Problems," *Progress in Aerospace Sciences*, Vol. 33, No. 9–10, 1997, pp. 539–586. doi:10.1016/S0376-0421(97)00001-8

[8] Jahnke, C. C., "On the Roll-Coupling Instabilities of High-Performance Aircraft," *Philosophical Transactions, Series A: Mathematical, Physical, and Engineering Sciences*, Vol. 356, No. 1745, 1998, pp. 2223–2239. doi:10.1098/rsta.1998.0271

[9] Liebst, B. S., "The Dynamics, Prediction, and Control of Wing Rock in High-Performance Aircraft," *Philosophical Transactions, Series A: Mathematical, Physical, and Engineering Sciences*, Vol. 356, No. 1745, 1998, pp. 2257–2276. doi:10.1098/rsta.1998.0273

[10] Jahnke, C. C., and Culick, F. E. C., "Application of Bifurcation Theory to the High-Angle-of-Attack Dynamics of the F-14," *Journal of Aircraft*, Vol. 31, No. 1, 1994, pp. 26–34. doi:10.2514/3.46451

[11] Lowenberg, M. H., "Development of Control Schedules To Modify Spin Behaviour," *AIAA Atmospheric Flight Mechanics Conference*, AIAA Paper 98-4267, 1998.

[12] Pashilkar, A. A., and Pradeep, S., "Computation of Flight Mechanics Parameters Using Continuation Techniques," *Journal of Guidance, Control, and Dynamics*, Vol. 24, No. 2, 2001, pp. 324–329. doi:10.2514/2.4715

[13] Ananthkrishnan, N., and Sinha, N. K., "Level Flight Trim and Stability Analysis Using Extended Bifurcation and Continuation Procedure," *Journal of Guidance, Control, and Dynamics*, Vol. 24, No. 6, 2001, pp. 1225–1228. doi:10.2514/2.4839

[14] Planeaux, J. B., Beck, J. A., and Baumann, D. D., "Bifurcation Analysis of a Model Fighter Aircraft with Control Augmentation," *AIAA Atmospheric Flight Mechanics Conference*, AIAA Paper 90-2836, 1990.

[15] Avanzini, G., and Matteis, G., "Bifurcation Analysis of a Highly Augmented Aircraft Model," *Journal of Guidance, Control, and Dynamics*, Vol. 20, No. 4, 1997, pp. 754–759. doi:10.2514/2.4108

[16] Goman, M. G., and Khramtsovsky, A. V., "Application of Continuation and Bifurcation Methods to the Design of Control Systems," *Philosophical Transactions, Series A: Mathematical, Physical, and Engineering Sciences*, Vol. 356, No. 1745, 1998, pp. 2277–2295. doi:10.1098/rsta.1998.0274

[17] Sinha, N., and Ananthkrishnan, N., "Use of the Extended Bifurcation Analysis Method for Flight Control Law Design," *AIAA Aerospace Sciences Meeting and Exhibit*, AIAA Paper 02-13591, 2002.

[18] Littleboy, D. M., and Smith, P. R., "Using Bifurcation Methods to Aid Nonlinear Dynamic Inversion Control Law Design," *Journal of Guidance, Control, and Dynamics*, Vol. 21, No. 4, 1998, pp. 632–638. doi:10.2514/2.4282

[19] Goman, M. G., Khramtsovsky, A. V., and Kolesnikov, E. N., "Evaluation of Aircraft Performance and Maneuverability by Computation of Attainable Equilibrium Sets," *Journal of Guidance, Control, and Dynamics*, Vol. 31, No. 2, 2008, pp. 329–339. doi:10.2514/1.29336

[20] Baghdadi, N., Lowenberg, M. H., and Isikveren, A. T., "Analysis of Flexible Aircraft Dynamics Using Bifurcation Methods," *Journal of Guidance, Control, and Dynamics*, Vol. 34, No. 3, 2011, pp. 795–809. doi:10.2514/1.51468

[21] Snell, S. A., Enns, D. F., and Garrard, W. L., Jr., "Nonlinear Inversion Flight Control for a Supermaneuverable Aircraft," *Journal of Guidance, Control, and Dynamics*, Vol. 15, No. 4, 1992, pp. 976–984. doi:10.2514/3.20932

[22] Shtessel, Y. B., and Shkolnikov, I. A., "Aeronautical and Space Vehicle Control in Dynamic Sliding Manifolds," *International Journal of Control*, Vol. 76, Nos. 9–10, 2003, pp. 1000–1017. doi:10.1080/0020717031000099065

[23] Singh, S. N., Steinberg, M. L., and Page, A. B., "Nonlinear Adaptive and Sliding Mode Flight Path Control of F/A-18 Model," *IEEE Transactions on Aerospace and Electronic Systems*, Vol. 39, No. 4, 2003, pp. 1250–1262. doi:10.1109/TAES.2003.1261125

[24] Saraf, A., Deodhare, G., and Ghose, D., "Synthesis of Nonlinear Controller to Recover an Unstable Aircraft from Post Stall Regime," *Journal of Guidance, Control, and Dynamics*, Vol. 22, No. 5, 1999, pp. 710–717. doi:10.2514/2.4439

[25] Raghavendra, P. K., Sahai, T., Kumar, P. A., Chauhan, M., and Ananthkrishnan, N., "Aircraft Spin Recovery, with and Without Thrust Vectoring, Using Nonlinear Dynamic Inversion," *Journal of Aircraft*, Vol. 42, No. 6, 2005, pp. 1492–1503. doi:10.2514/1.12252

[26] Atesoglu, O., and Ozgoren, M. K., "Control and Robustness Analysis for a High-α Maneuverable Thrust-Vectoring Fighter Aircraft," *Journal of Guidance, Control, and Dynamics*, Vol. 32, No. 5, 2009, pp. 1483–1496. doi:10.2514/1.42989

[27] Utkin, V. I., "Variable Structure Systems with Sliding Modes," *IEEE Transactions on Automatic Control*, Vol. 22, No. 2, 1977, pp. 212–222. doi:10.1109/TAC.1977.1101446

[28] Singh, S. N., "Asymptotically Decoupled Discontinuous Control of Systems and Nonlinear Aircraft Maneuver," *IEEE Transactions on Aerospace and Electronic Systems*, Vol. 25, No. 3, 1989, pp. 380–391. doi:10.1109/7.30793

[29] Hedrick, J. K., and Gopalswamy, S., "Nonlinear Flight Control Design via Sliding Methods," *Journal of Guidance, Control, and Dynamics*, Vol. 13, No. 5, 1990, pp. 850–858. doi:10.2514/3.25411

[30] Jafarov, E. M., and Tasaltin, R., "Robust Sliding-Mode Control for the Uncertain MIMO Aircraft Model F-18," *IEEE Transactions on Aerospace and Electronic Systems*, Vol. 36, No. 4, 2000, pp. 1127–1141. doi:10.1109/7.892663

[31] Seshagiri, S., Promtun, E., "Sliding Mode Control of F-16 Longitudinal Dynamics," *Proceedings of the American Control Conference* American Automatic Control Council, Evanston, IL, June 2008, pp. 1770–1775.

[32] Alwi, H., and Edwards, C., "Fault Tolerant Control Using Sliding Modes with On-Line Control Allocation," *Automatica*, Vol. 44, No. 7, 2008, pp. 1859–1866. doi:10.1016/j.automatica.2007.10.034

[33] Rao, D. M. K. K. V., and Sinha, N. K., "Aircraft Spin Recovery Using a Sliding-Mode Controller," *Journal of Guidance, Control, and Dynamics*, Vol. 33, No. 5, 2010, pp. 1675–1678. doi:10.2514/1.50186

[34] Doedel, E. J., Paffenroth, R. C., Champneys, A. R., Fairgrieve, T. F., Kuznetsov, Y. A., Oldeman, B. E.Sandstede, B., and Wang, X., "*AUTO2000: Continuation and Bifurcation Software for Ordinary Differential Equations (with HomCont)*," California Inst. of Technology, Technical Rept., Pasadena, CA, 2001.

[35] Paranjape, A. A., and Ananthkrishnan, N., "Airplane Level Turn Performance, Including Stability Constraints, Using Extended Bifurcation and Continuation Method," *AIAA Atmospheric Flight Mechanics Conference and Exhibit*, AIAA Paper 2005-5800, Aug. 2005.

[36] Goman, M. G., Khramtsovsky, A. V., and Kolesnikov, E. N., "Investigation of the ADMIRE Manoeuvring Capabilities Using Qualitative Methods," *Nonlinear Analysis and Synthesis Techniques for Aircraft Control*, edited by D. Bates, and M. Hadgstrom, Lecture Notes in Control and Information Sciences, Springer-Verlag, New York, Vol. 365, 2007, pp. 301–324.

[37] DeCarlo, R. A., Zak, S. H., and Matthews, G. P., "Variable Structure Control of Nonlinear Multivariable Systems: A Tutorial," *Proceedings of the IEEE*, Vol. 76, No. 3, 1988, pp. 212–232. doi:10.1109/5.4400

[38] Slotine, J. J. E., and Li, W., *Applied Nonlinear Control*, Prentice–Hall, Englewood Cliffs, NJ, 1991.

[39] Khalil, H. K., *Nonlinear Systems*, Prentice–Hall, Upper Saddle River, NJ, 2002.

[40] Gao, W., and Hung, J. C., "Variable Structure Control of Nonlinear Systems: A New Approach," *IEEE Transactions on Industrial Electronics*, Vol. 40, No. 1, 1993, pp. 45–55. doi:10.1109/41.184820

[41] Asseo, S. J., "Decoupling of a Class of Nonlinear Systems and Its Application to an Aircraft Control Problem," *Journal of Aircraft*, Vol. 10, No. 12, 1973, pp. 739–747. doi:10.2514/3.60299

[42] Lane, S. H., and Stengel, R. F., "Flight Control Design Using Non-Linear Inverse Dynamics," *Automatica*, Vol. 24, No. 4, 1988, pp. 471–483. doi:10.1016/0005-1098(88)90092-1